JOURNAL OF GEOPHYSICAL RESEARCH, VOL. 99, NO. E10, PAGES 21,153–21,171, OCTOBER 25, 1994

Bell Regio, Venus: Integration of remote sensing data and terrestrial analogs for geologic analysis

Bruce A. Campbell
Center for Earth and Planetary Studies, National Air and Space Museum, Washington, D.C.

Patricia G. Rogers
Solar System Exploration Division, NASA Headquarters, Washington, D.C.

Abstract. The geology and surface morphology of Bell Regio (18-42° N, 32-58° E) are investigated using a combination of Magellan, Venera, and analogous terrestrial data. The properties of surface units are compared to either direct terrestrial analog measurements or to the behaviors predicted by theoretical models. Five major volcanic sources are identified from geologic mapping (Tepev Mons, Nefertiti corona, a large shield volcano east of Tepev, and two small edifices southeast of Tepev). The volcano Api Mons lies northeast of the main Bell uplift. The oldest volcanic units are associated with an extensive low shield volcano east of Tepev Mons and a small edifice southeast of Tepev. The annular flow apron of Tepev Mons formed next, with volcanism at a second small edifice on the southeast flank of Tepev Mons producing the youngest flow units. Comparisons between Magellan data, terrestrial radar images, and field topography profiles suggest that only three units resemble terrestrial a'a flows; the remainder are consistent with smoother pahoehoe-type surfaces. This suggests that most of the flow units were erupted at relatively low volume effusion rates (<100 m^3/s) over long periods of time or had very low viscosities. One flow unit has a knobby texture which resembles large tumuli or ridge structures. Much of the tectonic deformation in the area is in the form of fractures circumferential to the edifices and isolated blocks of tessera terrain; there are no rift zones such as those which occur at Beta Regio, Atla Regio, or Western Eistla Regio. Tepev Mons is characterized by very steep slopes (up to 40° along the east flank), a relatively flat summit, and two large (11 and 31 km) calderas. Though covered in places by high-dielectric material, the Tepev Mons summit area is relatively smooth with the exception of annular rough deposits which ring the two calderas. These calderas are quite shallow (on the order of a few hundred meters at most), with no discernible difference in radius between individual altimeter footprints inside and outside the larger eastern feature. Magellan and Venera data suggest that the eastern caldera is covered by a layer of unconsolidated material. Ejecta from Miriam crater has produced a halo with a dielectric constant of 6-7 surrounding Nefertiti corona, and Potanina crater ejecta is the likely source material for radar-dark wind streaks south of Tepev Mons. A low-dielectric (ε=2-3) triangular region on the south flank of Tepev Mons may be a pyroclastic or crater ejecta deposit which has been spread westward by the wind. This region has undergone a wide variety of volcanic processes, with a major shift in eruptive style from the older low-relief eastern volcanic center to the steep slopes and large summit calderas characteristic of Tepev Mons and the two smaller edifices.

Introduction

Large volcanic structures on Venus are important indicators of mantle-lithosphere interaction and, in some cases, the long-term development of hotspot plumes and associated magma reservoirs. The edifices and their lava flows permit development of regional stratigraphic sequences and a better understanding of volcanic evolution than the more extensive, but often featureless, plains. To understand the styles of lava flow emplacement and the formation of large Venusian edifices, it is important to carry out detailed studies of the shape, distribution, stratigraphic relations, surface morphology, and bulk properties of their volcanic deposits. In this paper, we use a combination of Magellan and Venera datasets to characterize Bell Regio, a volcanic rise located at 30° N, 45° E (Figure 1).

Previous studies of Bell Regio have been relatively limited. This upland is outside of the coverage provided by Arecibo images, and Venera data extend southward only to the central portion of the largest edifice, Tepev Mons. Much of the earlier work focused on characterizing the nature of isostatic compensation beneath Tepev Mons, concluding that some form of dynamic support (i.e., a hotspot plume) is required to explain the gravity signature of this mountain. The geology and geophysics of the region have been discussed by *Janle et al.* [1987, 1988], but these analyses were hampered by the limited image coverage and a reliance on coarse-resolution Pioneer-Venus (PVO) altimeter data for gravity modeling

Paper number 94JE01862.

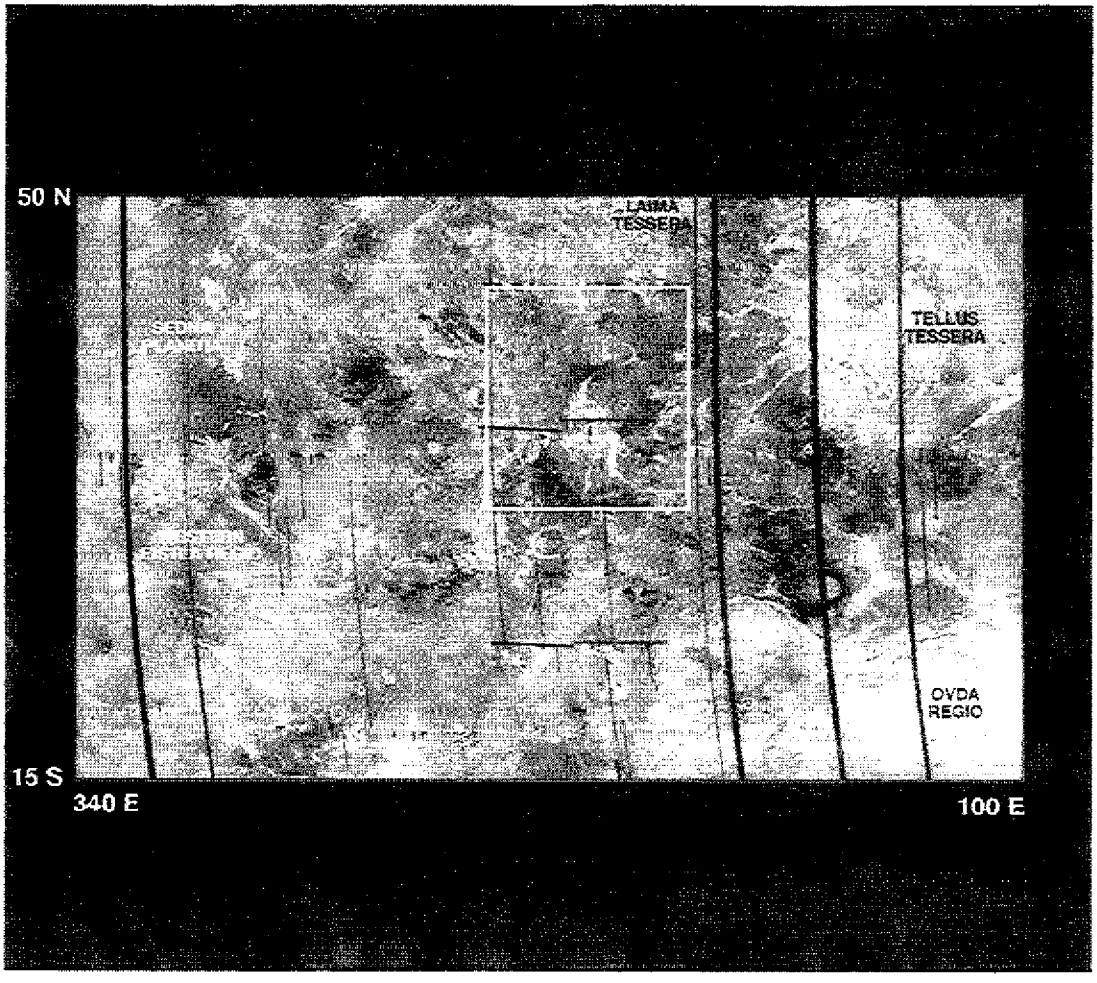

Figure 1. Location map showing relationship of the Bell Regio study area, outlined by the white box (18-42°N, 32-58°E), to other Venus features. Mercator projection of Magellan SAR data.

[*Campbell and Kozak*, 1988]. *Smrekar and Phillips* [1991] included Tepev Mons in a study of the gravity signatures of volcanic edifices, and more recent work [*Solomon et al.*, 1992; *Senske et al.*, 1992; *McGovern and Solomon*, 1992] has used Magellan data to place Bell Regio within a global framework of large volcanic rises. New Magellan circular-orbit gravity data will greatly improve the estimates of compensation for the region [*Konopliv et al.*, 1993; *Smrekar*, 1994]. The detailed stratigraphy and geologic evolution of the area remain to be analyzed.

To characterize the extensive volcanic and tectonic features which comprise Bell Regio, we use Magellan synthetic aperture radar (SAR) imagery, altimeter measurements of topography and rms slope, emissivity measurements, and Venera 15/16 SAR data. Magellan SAR images are the primary tool for unit definition and geologic mapping. AIRSAR data for Hawaiian lava flows are used to infer volcanic surface morphology from Magellan backscatter data, and field topography profiles provide a guide to the interpretation of Magellan altimeter rms slope measurements [*Campbell and Campbell*, 1992; *Campbell and Garvin*, 1993]. A model that relates Magellan emissivity and SAR backscatter data to dielectric constant and roughness values is used to constrain the variability of bulk permittivity across the Venus surface [*Campbell*, 1994]. Taken together, these techniques permit a comprehensive characterization of the geologic units mapped from the SAR images. This multifaceted study is intended to (1) provide the first detailed description of the geology and evolution of Bell Regio, and (2) demonstrate techniques for integrating Magellan data sets with other sources of information to enhance geologic analysis.

By studying Magellan data and terrestrial analogs, a number of questions regarding volcanism and radar scattering on Venus can be addressed, including (1) what are the distributions of volcanic deposits (the primary geologic units) in Bell Regio, where are their likely source vents, and what is the general stratigraphic succession within the region?; (2) what are the surface morphologies of the lava flows, and what do these results indicate about eruption rates and styles?; (3) what is the nature of the low-emissivity deposits on the mountaintops, and are there spatial variations in roughness within these units?; (4) what kind of surface changes accompany the variations in plains radar brightness within this region?; (5) what is the structure of the Tepev Mons calderas?; (6) what processes caused the halo of anomalous emissivity surrounding Nefertiti, and are there other significant dielectric variations within this region? Each of these questions will be addressed using a combination of

spacecraft data and terrestrial analogs or theoretical models, and at each stage the utility and difficulties associated with these techniques are discussed.

We first present a geologic map of the study region and discuss the basic stratigraphy of volcanic, impact crater, and tectonic features. The Magellan measurements of backscatter, rms slope, and emissivity are then used to characterize the surface morphology and bulk dielectric properties of the area, and to augment the geologic interpretations made from the SAR-derived unit map. The individual radar altimeter footprints for the Tepev Mons summit are analyzed to extract the maximum information on local topography and surface properties. Finally, we summarize the remote sensing results in the context of the geology of the region, and discuss the possible nature of anomalous surface features.

Regional Geology of Bell Regio

Bell Regio (18-42° N, 32-58° E) is a broad rise, approximately 1500 km in diameter, which is characterized by extensive volcanism centered on several edifice complexes (Figure 2). Within the main highland region of Bell Regio we have mapped five major volcanic sources: Tepev Mons, Nefertiti corona, an unnamed volcano east of Tepev, and two small, steep edifices on the southeast flank of Tepev. The shield volcano Api Mons and several coronae with associated flow fields occur nearby. To assess the sequence of events and the styles of lava flow emplacement, we produced a geologic map (Plate 1). Unit boundaries were defined primarily on the basis of changes in radar backscatter cross section, surface morphology, and structure. The mapped units can be placed within a tentative relative age sequence based on superposition and cross-cutting relationships, shown in Figure 3. We discuss each of the units below.

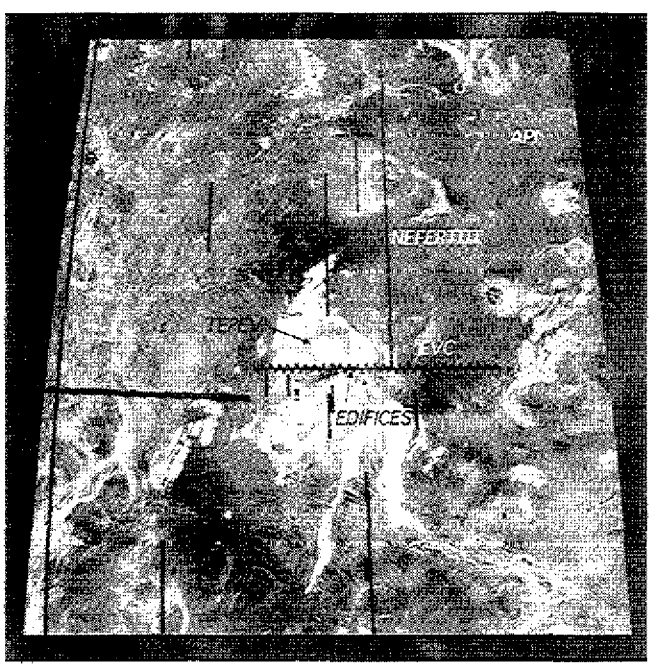

Figure 2a. Magellan radar image of Bell Regio. Image is in a sinusoidal projection, with a resolution of 1.2 km. Image boundaries 18°-42°N, 32°-58°E. "EVC" indicates the large eastern volcanic center. Api Mons, Nefertiti Corona, and two small edifices on the southeast flank of Tepev Mons are also indicated.

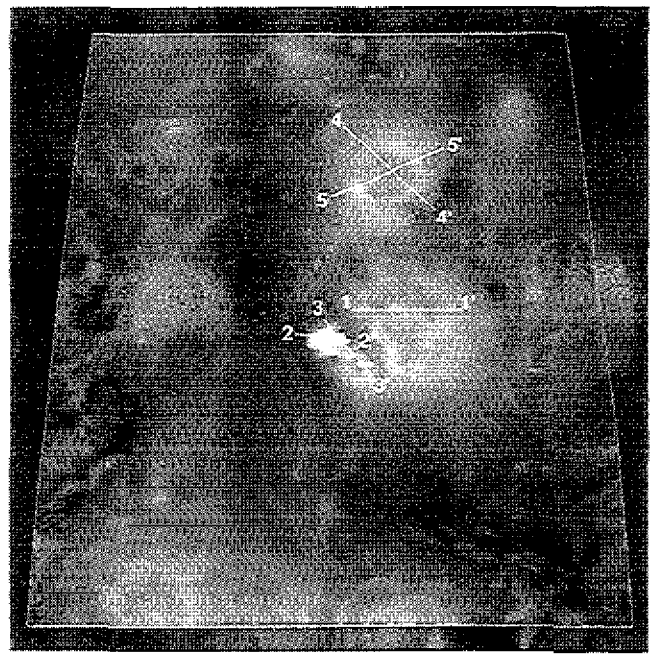

Figure 2b. Gray-scale rendering of Magellan topography for the same area. Data from global average data set (spatial averages at 5-km pixel spacing). Areas lower than -400 m relative to the 6051.0-km datum shown as black; areas above +5800 m shown as white. Topographic profiles 1-5 discussed in text are indicated on the map; the unprimed and primed labels indicate the start (left) and end (right) points in profile traces.

Tessera

There are a number of radar bright tectonic units which rise above the surrounding plains and are deformed in multiple directions (tessera). All tessera (Unit *t*) regions are embayed by later lava flows, indicating that these are the relatively oldest units. Large tessera blocks lie east, west, south, and north of Tepev Mons, and all are oriented along a SW-NE trend. The 700-km-long eastern tessera unit contains fractures that are less regularly oriented than those associated with the other three major occurrences.

Plains

The terrain surrounding Bell Regio is dominated by plains, which we have subdivided into three major units. The first type, radar-dark plains (*dp*), are found to the north, west, and southwest of Tepev Mons. The second type, extensive radar-bright plains (*lp*), surround virtually the entire highland region. Both of these units contain E-W or SE-NW fracture patterns, and differ only in their relative radar brightness. The dark plains in most cases appear to be areas where smooth lava flows have flooded a preexisting light plains unit, and in at least one case (between Tepev Mons and Nefertiti) the dark material overlies flow aprons from the major volcanic centers. The third unit, ridged plains (*rp*), is comprised of more heavily deformed regions with two or more overlapping patterns of ridges. The dominant lineament patterns are oriented SE-NW and SW-NE.

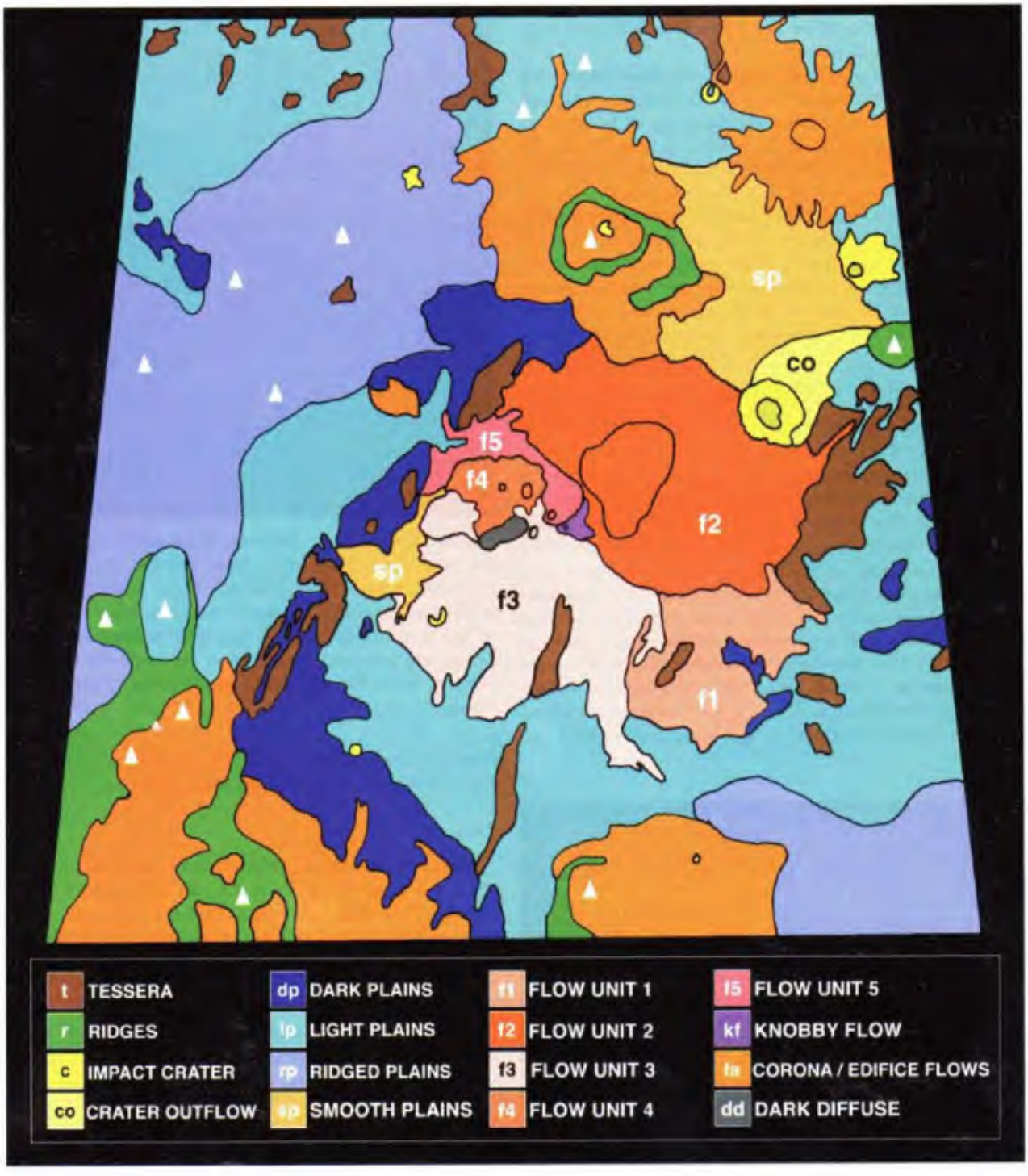

Plate 1. Geologic map of Bell Regio. Area and map projection identical to that of Figure 1. Legend indicates geologic unit types. White triangles mark the approximate centers of coronae and annular tectonic features. Black outlines within geologic units mark calderas, crater interiors, small edifices, and steep-sided domes. The radar-bright oval area within unit *f3* is differentiated from the rest of the flow complex by a black boundary.

These groupings of plains, often characterized by the nature of their tectonic structures, points out a difficult issue in mapping from SAR data: many units are differentiated only by the density and orientation of ridges, graben, or other bright lineaments. Since the goal of geologic mapping is to define distinct rock units, the degree of deformation should not neccesarily dictate their boundaries, but the gross difference in the appearance of these plains dictates some recognition on the map.

Eastern Volcanic Center (EVC)

The earliest episode of edifice-forming volcanism in Bell Regio occurred on a large shield volcano located between Tepev Mons and Potanina crater. This volcano is characterized

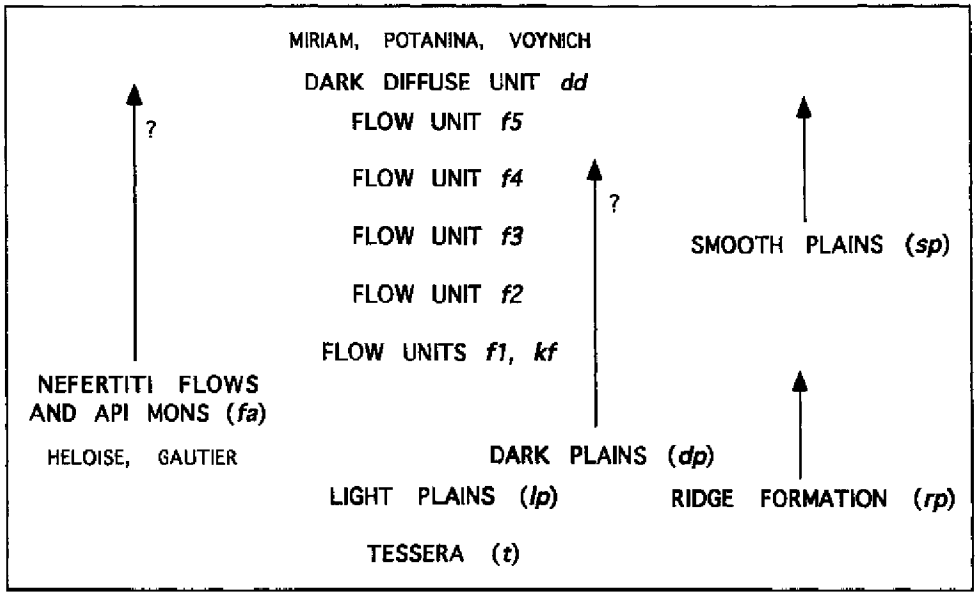

Figure 3. Preliminary stratigraphic sequence for mapped units. Youngest deposits are at the top, oldest toward the bottom. Arrows indicate events which extended over significant periods. Note the uncertainty in the relative timing of Nefertiti corona, Api Mons, and Tepev Mons flow units. Craters are denoted by smaller letters.

by gentle flank slopes (typically less than 1°), a central bulge surrounded by a topographic moat and a wishbone pattern of ridges, and a prominent radial pattern of pit crater chains (Figure 4). Circumferential fractures occur to the east, south, and northwest of the central pit crater area.

Figure 4a. Magellan SAR image of eastern volcanic center. Image width ~350 km, centered on 29.9°N, 48.5°E.

There are three major lava flow complexes associated with the eastern volcanic center. Flow Unit 1 (*f1*) is a moderate to low radar return flow field that embays the ridged plains and tesserae to the south and extends radially up to 600 km from the center of the EVC. Large portions of Flow Unit 1 proximal to its inferred source are buried by the deposits which make up Unit 2. This later complex of flows (*f2*) radiates from the EVC and extends up to 450 km. In general, Unit 2 flows are more radar-dark than those of Unit 1. The eastern portions of this complex are marked by isolated bright flow margins which may represent the transition of smooth, broad lava flows to rougher, more distinct lobate structures; these lobes may also be higher-standing, embayed Unit 1 flows.

Flow Unit 3 (*f3*) is a prominent aggregate of radar-bright lava flows to the south and southwest of Tepev Mons. Many of these flows are emplaced radial to the large eastern volcanic center, and some appear to have erupted from concentric fractures on the flanks of the edifice. To the southeast of Tepev Mons, these bright flows are superposed on the earlier radar-

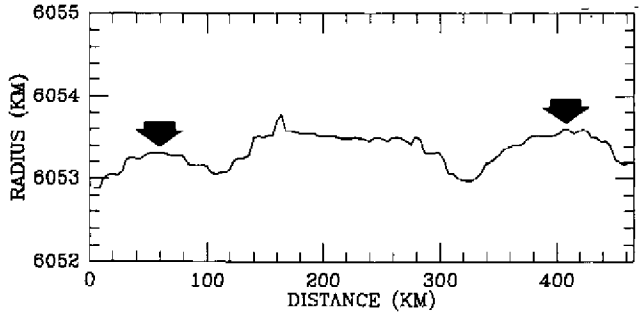

Figure 4b. Topographic profile through this area (location shown on Figure 2b as profile 1). Note the interior bulge, flanking moats, and symmetric outer ridges (shown by arrows).

Figure 5. Magellan SAR image of ponded lava south of Tepev Mons. Image width ~230 km, centered on 24.4°N, 44.7°E. White arrows indicate large wind streaks; black arrow indicates south margin of lava delta.

dark deposits of Units 1 and 2. Unit 3 flows erupted from a number of source vents, but we have grouped them together due to similarities in radar brightness and relative age. Within this flow complex there is a region of ponded lava (~140-km diameter, centered at 24.5°N, 44.5°E) with a 40 km lava delta along its north margin (Figure 5). A 230-km channel debouches into the ponded area after passing through the lava delta. There are numerous small volcanic constructs within the radar-dark ponded lavas, but it is unclear whether these cones or the flows which created the channel are the major contributors to the ponded material.

Small Edifice I

On the southeast flank of Tepev Mons is a 4.9-km (above the 6051.0 km datum) edifice which appears to have erupted prior to or contemporaneous with the eastern volcanic center (Figure 6). This steep (20-40° flank slope) volcanic source is centered in a Magellan data gap, and only one altimeter measurement constrains its height. It is clear from the very bright radar return near the summit (also seen in PVO image data) that the altitude must be greater than −6053 km, based on similar enhancements with altitude elsewhere on the planet [*Klose et al.*, 1992]. Immediately southwest of the edifice are a set of scarps and adjacent hummocky terrain which appear to be the collapsed margin of a steep-sided dome. A dark lava flow emanates from the base of the exposed flank. A second (31-km-diameter) steep-sided dome is located just west of this feature, and is partially buried by later flows. The two domes may have formed at approximately the same time.

A triangular lava flow (Unit *kf*) extends to the east of the Edifice I peak, and is covered or embayed in many places by later flows from the EVC and the small volcano to the northwest. The portions which show through are quite rough at scales of several hundred meters, with structures that are knobby in some locales and ridge-like in others. This relatively old unit may have formed by eruption of highly viscous magma, similar to the festooned flow studied by *Moore et al.* [1992], or by slow inflation of a tumuli field by more ordinary basaltic magma [*Theilig and Greeley*, 1986]. The association of such a flow, the steep edifice, and the adjacent dome offers a view of several features which are uncommon on Venus.

Tepev Mons

Tepev Mons is a 300-km-diameter shield volcano with a complex summit area comprised of overlapping flow sequences and two large (11-and 31-km-diameter) circular

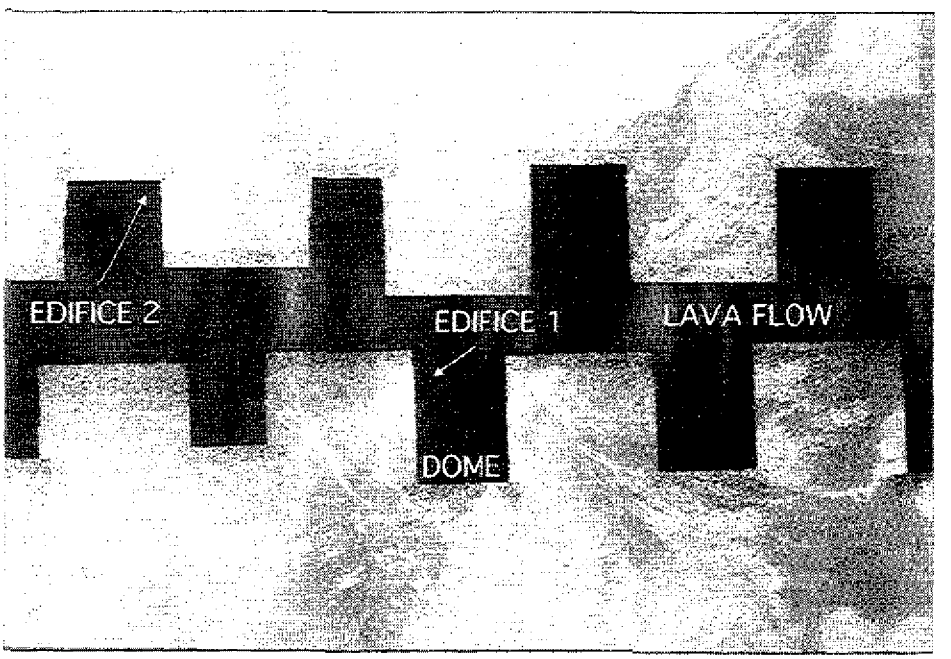

Figure 6. Magellan SAR image of edifice I, edifice II, and the collapsed dome and rough flow discussed in text. Image width ~130 km, centered on 28.7°N, 46.7°E. Note the circular feature atop edifice II and the knobby or ridged structure of the eastern lava flow.

features (Figure 7). The summit features are likely calderas, though neither shows the bright return expected from steep radar-facing crater walls. This may suggest shallow or infilled structures similar to that found at Sif Mons. Both calderas are surrounded by material with very high radar return, consistent with the presence of high-dielectric materials at these elevations [*Klose et al.*, 1992]. The echoes from the caldera floors are much less enhanced, and we will address this observation below. The flanks of the shield are characterized by slopes of 20-40°, which are quite steep in comparison to many other volcanoes on Venus (Figure 7c). There is a well-defined pattern of radar-bright fractures circumferential to the central peak of Tepev Mons, with a few smaller radial tectonic features. Collapse pits and pit crater chains are located near the summit, and some may have been vents for volcanic material.

Flow Unit 4 (*f4*) is composed of narrow interfingered radar-bright and dark lava flows which form an apron around Tepev Mons. These flows radiate ~200 km from the summit of the edifice, and presumably were erupted from the calderas or from nearby pit craters or fractures. Since there is no clear contact between these flows and the deposits of the eastern volcanic center, we cannot establish the relative age of units *f3* and *f4*.

Small Edifice II

A second "small" edifice (4.4 km) occurs southeast of Tepev Mons (Figures 2, 7c). Activity centered on this construct produced a series of radar-bright flows (*f5*) that are superposed on units *f2* and *f4*. Unit 5 encircles the Tepev summit apron and embays portions of a tessera unit to the north. *McGovern and Solomon* [1992] suggested that these flows follow and infill a topographic moat formed due to lithospheric loading, and the data in Figure 7c appear to suggest such a depressed region north of Tepev Mons. The south margin of the E-W trending bright lava flow, shown in Figure 8, provides clear evidence that Unit 5 superposes the Tepev apron. If the Unit 4 lavas were younger than the bright flow, we would expect to see either embayment of the rough flow at low areas or ponding of smooth material against the flow margin. The absence of any such features suggests that *f5* overlies *f4*. Portions of unit *f5* also embay the knobby flow unit from small edifice I.

Not all of the *f5* lava flows may have erupted from small edifice II. One large pit crater chain on the north flank of Tepev appears to have erupted some amount of lava, which flowed down the adjoining graben into the topographic depression surrounding the volcano. There are also small flows northwest of edifice II which may have come from nearby pit crater chains.

Other Flow Complexes

Two areas within the study region are characterized by smooth fields of lava with no lobate structures, few fractures, and no abrupt changes in radar brightness. These deposits, labeled as Unit *sp*, differ from the other plains units in being younger and evidently associated with the edifices, but lack the lobate structures seen in the major flow complexes (*f1-f5*, *kf*). The northeast unit is centered on a field of small domes (<10 km diameter) which are the likely source vents for the eruptions. The western deposit appears to flood a light plains

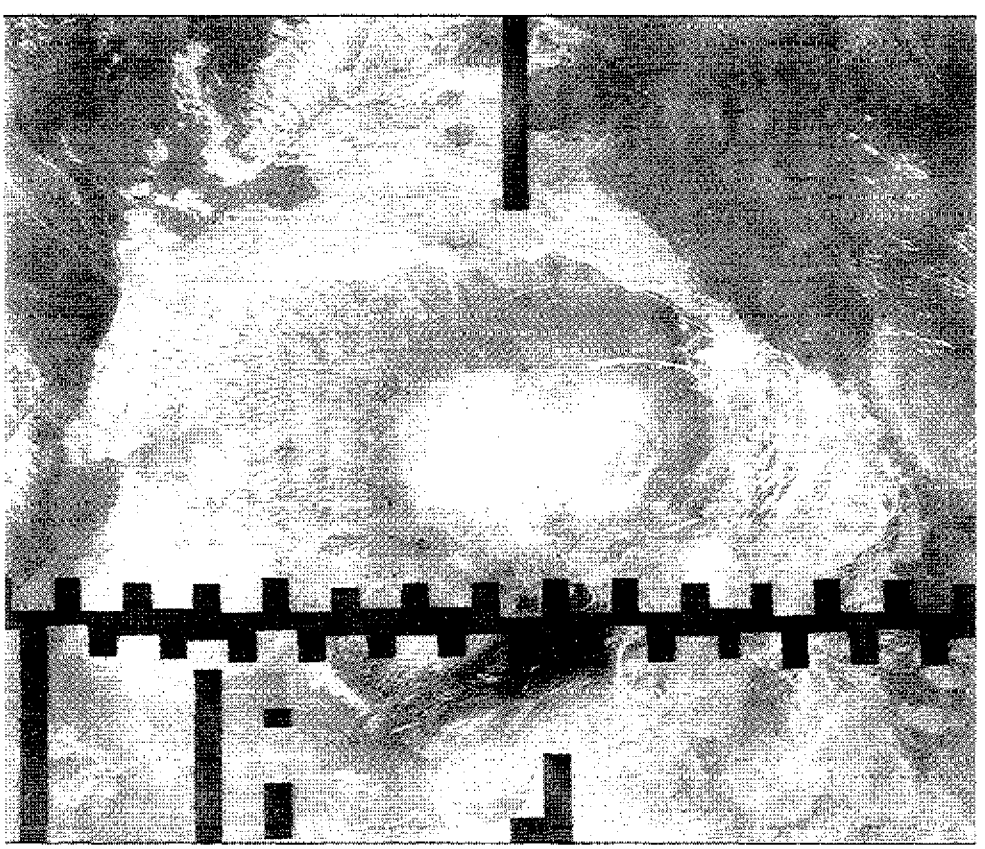

Figure 7a. Magellan SAR image of the Tepev Mons summit area. Image boundaries 27.6-31.9°N, 42.0-47.6°E.

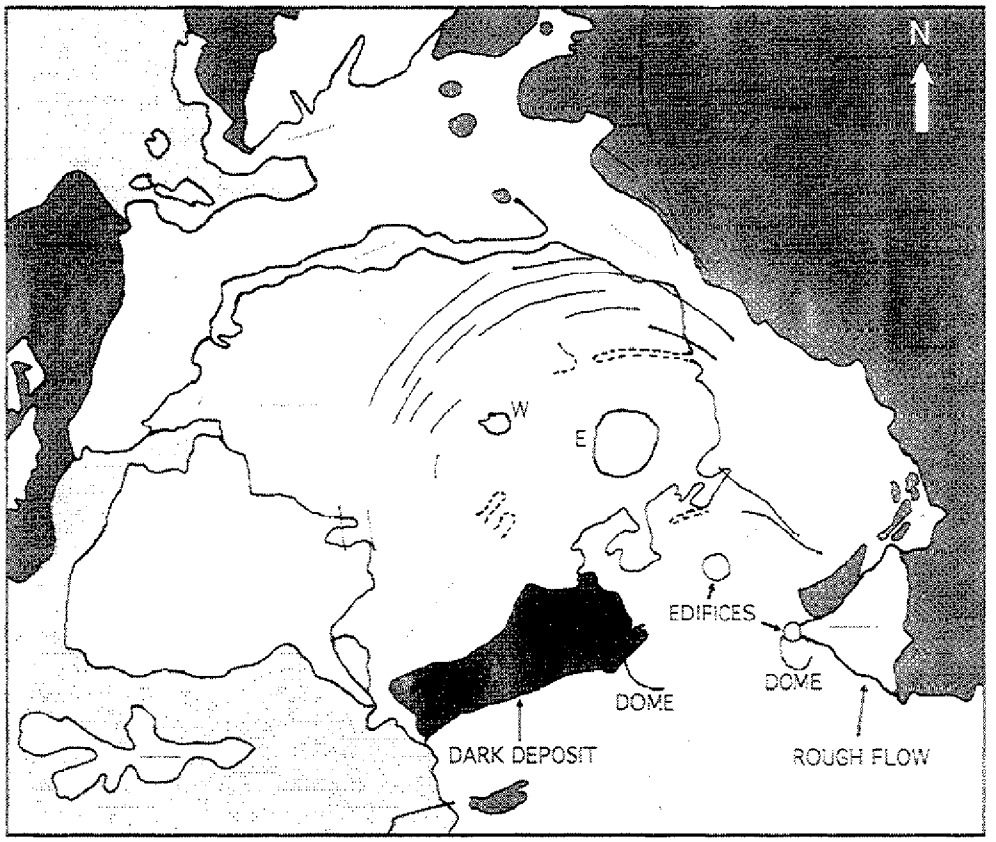

Figure 7b. Sketch map of geologic features for the identical area in Figure 7a. Tessera, light plains, dark plains, and the dark diffuse deposit are shown by progressively darker gray tones. Lava flow units related to Tepev Mons and the two smaller edifices are left white in this map. W and E denote the locations of the western and eastern Tepev Mons calderas. Solid black lines indicate major fractures; note that most are concentric to Tepev Mons and the eastern volcanic center. Gray arrows indicate lava flow directions. The bright flow which circles the north portion of the Tepev lava apron (unit *f4*) is part of the larger *f5* unit, but we have indicated its margins where the roughness becomes much greater than that of the surrounding flows.

unit, but the source for these flows is uncertain. Lobate flow fields from coronae and edifices not contiguous with the main portion of Bell Regio (i.e., Api Mons) are indicated by Unit *fa* on the map.

Coronae

There are a variety of features within the study area whose patterns of radial and annular fractures fit the description of coronae. Nefertiti corona is the largest such feature in Bell Regio (500 x 230 km in diameter, centered at 36°N, 48°E), with a central depression surrounded by broad topographic highs (Figure 9). The eastern portion of the corona appears to have moved due to gravity-sliding ~200 km toward the southeast, as evidenced by the rapid drop in elevation along the corona margin and the displaced ridges. Radial volcanic flows extend at least 120 km from the eastern and northern rim of Nefertiti and cover portions of the ridged plains. Small domes and calderas (<10 km in diameter), associated bright flows, smooth plains, and linear ridges and fractures are evident in the interior of Nefertiti, consistent with *Stofan et al.'s* [1992] classification of this as a Category 3 corona. The flow complex from Nefertiti superposes the light plains, but there is no clear relationship to the EVC or Tepev Mons lava flows.

Two large coronae occur at the south edge of the study area, and both have lava flow aprons similar to that found at Nefertiti. A 160-km-diameter corona lies west of Tepev Mons (27°N, 34.5°E), but volcanism at this site is confined to small radar dark patches within the central area. Many smaller coronae are found in the heavily ridged plains to the west of Bell. In general, they cannot be separated in terms of relative age from the general deformation of these regions. We have mapped features with obvious associated volcanism and major ridge boundaries (e.g., Nefertiti) as discrete units, with unit type *r* indicating the heavily ridged margins. We have included those features defined only by tectonic patterns within the highly deformed plains category. The approximate center of each corona or annular feature is indicated by a white triangle symbol on the map.

Impact Craters

Eight impact craters and their associated deposits are mapped (Unit *c*). The most distinct are Potanina (31.7°N, 53.1°E, 90-km diameter), Voynich (33°N, 56°E, ~50-km diameter), and Corinna (22.9°N, 40.4°E, 20-km diameter). Potanina has a long outflow deposit (Unit *co*) which extends 260 km northeast from the edge of the continuous ejecta blanket. To the southwest of Tepev Mons (26.5°N, 42.8°E) the

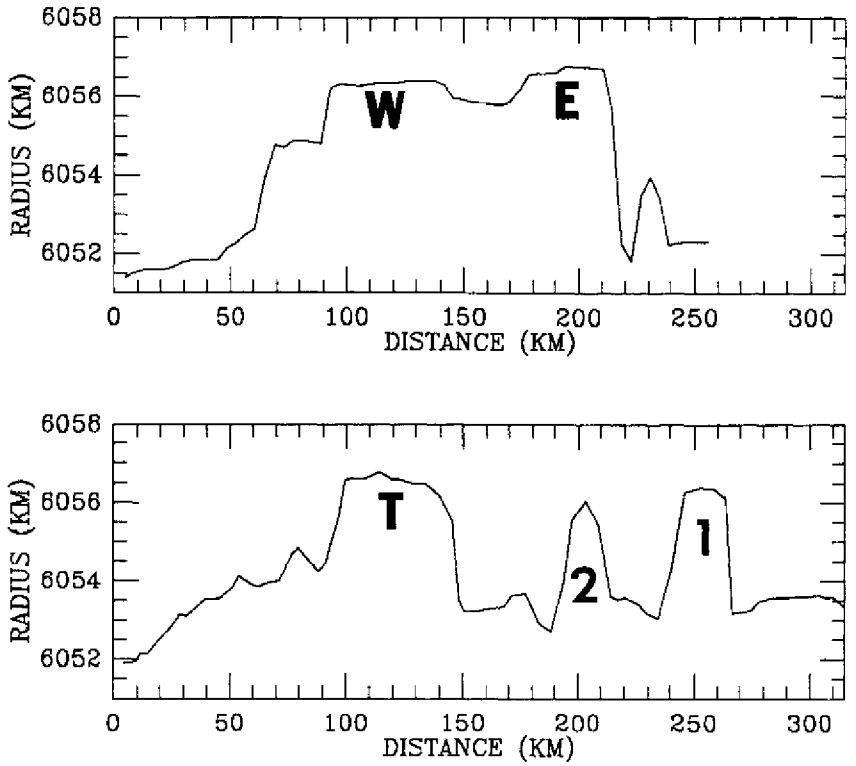

Figure 7c. Topographic profiles through this region (locations shown on Figure 2b). Profile 2 crosses Tepev Mons, and the locations of the western and eastern caldera are noted. Profile 3 shows Tepev Mons and the two small edifices, indicated by T, 1, and 2 on the plot. Note the very steep slopes (20-40°) on all three constructs.

60-km-diameter crater Gautier has been largely buried by lava flows, and the small horseshoe feature Heloise northwest of Api Mons also appears to be a flooded crater. The 13-km-diameter bright-floored crater Miriam lies inside Nefertiti corona.

Crater ejecta has produced a number of important surface features. Surrounding Potanina and Miriam are numerous patches of dark terrain, inferred to be deposits of fine-grained material which mantles the underlying surface and reduces the backscattered return. There are also radar-dark windstreaks near the tessera unit south of Tepev Mons (Figure 10), produced by movement of fine-grained ejecta material (presumably from Potanina) from the tessera onto the nearby plains. The linear dark streaks are often aligned with gaps in the outer tessera

Figure 8. Magellan SAR image of bright lava flow north of Tepev Mons flow apron. Image width ~125 km, centered on 30.5°N, 43.8°E. Black arrows indicate examples of dark lava flows (*f4*) truncated by the younger bright flow (*f5*).

Figure 9a. Magellan SAR image of Nefertiti corona. Image width ~680 km, centered on 36.2°N, 48.0°E. White arrows indicate radar-dark wind streaks and pile-ups of fine-grained crater ejecta; black arrow indicates Miriam crater.

margin, consistent with debris which has been funneled between topographic obstacles. The long arcuate dark streaks to the west superpose the ponded lavas discussed above. Similar dark wind streaks are found east and southeast of Nefertiti, where they mix with ejecta from Miriam (Figure 9a). This dark material forms linear or wispy features [*Greeley et al.*, 1992], and often appears to pile up against topographic obstacles to form low-return shadows along ridges or hills. There is also a radar-bright deposit west of Nefertiti apparently produced by Miriam.

A roughly triangular area of low radar backscatter with feathery margins (*dd*) occurs just south of the summit of Tepev Mons and widens toward the west (Figure 7). This dark material appears to completely blanket the adjacent lava flows at the northeast apex of the triangle, and thins out to expose more of the underlying terrain as the deposit widens. There is no crater-like feature or bright central region to this deposit, and we will discuss its possible origin in more detail below.

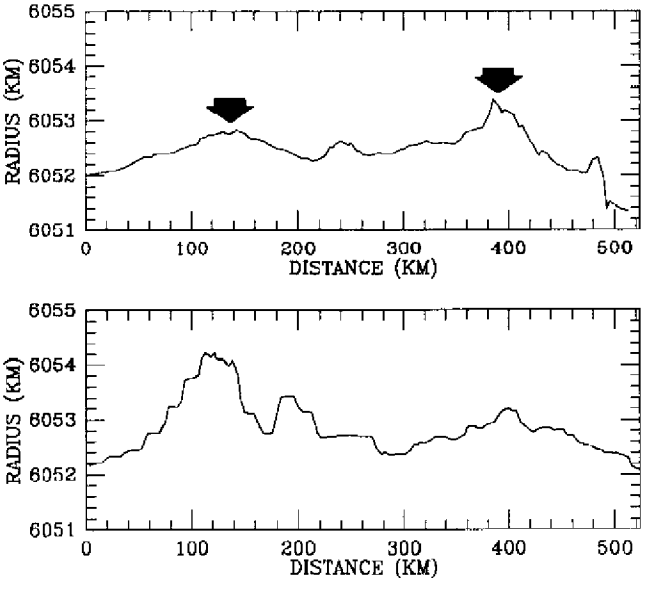

Figure 9b. Topographic profiles (indicated as profiles 4-5 on Figure 2b) through this region. Profile 4 shows the symmetric ridge structure (arrows) and the central depression. Note the abrupt drop in elevation to the east, where the SAR image shows apparent slumping of the corona rim. Profile 5 shows the maximum elevations along the southwest corona margin.

Figure 10. Magellan SAR image of wind streaks near tessera block south of Tepev Mons. Image width ~175 km, centered on 23.4°N, 46.2°E. White arrows indicate radar-dark wind streaks.

Analysis of Surface Properties

The preceeding section presented a geologic interpretation of Bell Regio based primarily on mapping using SAR images and large-scale topography data. Such an approach permits the distribution and relative age of major geologic units to be defined, but it does not provide a detailed analysis of the roughness and dielectric properties of surface materials. A frame of reference with respect to similar terrestrial features (i.e., lava flows) is also needed. In this section, we analyze the backscatter properties of units mapped in Bell Regio using Magellan and Venera 15/16 data, and compare these radar characteristics to those of terrestrial lava flows and predictions from theoretical scattering/emission models.

Magellan Backscatter Versus AIRSAR Backscatter

To understand the radar scattering behavior of lava flows on Venus, we can make direct comparisons between Magellan backscatter coefficient (σ_o) values and synthesized S-band (12.6-cm) AIRSAR echoes for Hawaiian lava flows [*Arvidson et al.*, 1992; *Campbell and Campbell*, 1992]. Magellan SAR data have an incidence angle range over Bell Regio of 37°-45° [*Saunders et al.*, 1992]. Nineteen sample regions were selected within the study area, and their locations are indicated on Figure 11. For each site, we calculated the average backscatter coefficient and altimeter-derived rms slope (Table 1). If we compare σ_o values for the Bell Regio sites to those for six Hawaiian lava flows (Figure 12), we find that many of the plains units (*dp* and *lp*) are quite radar-dark compared to even a smooth terrestrial basalt. The lowest radar return shown for the Hawaiian lava flows corresponds to a surface with an rms

Figure 11. SAR backscatter analysis sample areas, with numbers keyed to Table 1, outlined on radar image of Bell Regio. Actual sample data averaged over a C1-MIDR image (225-m resolution).

height of only 1-2 cm, so the dark Venus areas must be either exceedingly smooth or covered in part by a thin soil.

Values of σ_O comparable to those of terrestrial transitional or a'a (-9 dB<σ_o(40°)) flows are shown in a yellow-red stretch in Plate 2. Most of the flow fields and plains in this region are similar in roughness to Hawaiian pahoehoe flows. Only three large a'a-type surfaces are identified: (1) a flow north of Tepev Mons which rings unit *f4*; (2) the bright oval flow region west of Tepev Mons; (3) a large flow (part of *f3*) which extends south from the fractures concentric to the eastern volcanic center. There are also numerous small lava flow areas with high roughness. The tessera and the ejecta blanket of Voynich are quite rough, presumably due to abundant rock fragments. Portions of the summit of Tepev Mons are much brighter than even a very rough terrestrial lava flow, suggesting enhanced Fresnel reflectivity. The calderas atop Tepev Mons (Figure 7) are noteable for having backscatter cross sections much lower than those found in the surrounding haloes; their absolute brightness is similar to that of rougher Hawaiian pahoehoe flows (Table 1). The bright halo surrounding the eastern caldera decreases in backscatter strength as we move from west to east around the rim; this effect is likely an artifact of the steep slope on the east side of the volcano, which tilts the ground away from the left-looking radar system.

Table 1. Site Number (Keyed to Figure 11), Description and Map Unit Designation, Number of Radar Datapoints Within Box, Average Radar Backscatter Coefficient, Number of Altimeter Footprints Within Box, and Mean rms Slope for Sample Areas

Site	Description (Unit)	*N*radar	Mean σ_o, dB	N_{rms}	Mean ϕ_{rms}, deg
1	N. Tepev flow (*f5*)	3332	-8.1	2	8.9
2	N. Tepev flow (*f5*)	7018	-10.5	2	6.5
3	E. Caldera floor	6351	-11.0	2	8.6
4	W. Caldera floor	713	-9.4	0	-----
5	Tepev bright halo	696	-1.9	1	2.4
6	W. bright flow (*f3*)	3690	-9.5	3	1.6
7	NW Tessera (*t*)	23707	-10.3	8	7.8
8	S. bright flow (*f3*)	6840	-8.1	4	6.0
9	SW dark plains (*dp*)	63024	-24.1	20	1.3
10	SW light plains (*lp*)	24186	-19.7	11	0.9
11	N dark plains (*dp*)	48393	-23.5	14	1.5
12	Nefertiti halo	19019	-14.3	8	2.2
13	E. dark flows (*f2*)	199172	-20.8	22	2.1
14	Dark diffuse unit (*dd*)	7209	-24.0	2	1.1
15	NW dark plains (*dp*)	23961	-19.9	8	1.2
16	NW light plains (*lp*)	72782	-18.1	23	1.5
17	S. lava field (*f3*)	93906	-11.5	27	2.9
18	Lava delta (*f3*)	81830	-19.5	32	0.8
19	Tepev lava apron (*f4*)	54750	-13.2	15	3.6

Radar data averaged at the C1-MIDR (225 m) scale.

Magellan Backscatter Versus Venera 15/16 Data

The Venera 15/16 spacecraft collected right-looking radar images with an incidence angle of ~10° for the region north of about 30° latitude. These data must be interpreted with caution because they were processed with an automatic gain control which high-pass filtered the imagery, thus eliminating any opportunity to compare backscatter variations on large spatial scales. Over small areas, however, the Venera data can be used to study boundaries between geologic units. The Venera image (Figure 13) is contrast-reversed with respect to Magellan data in most areas, since at this incidence angle the strongest echoes are those from smooth surfaces with large quasi-specular returns. These data provide a better view of small edifice I than can be derived from Magellan images. The radar-dark area to the west of the mountain is larger than that found for edifice II, confirming that this feature is likely taller and has steep flank slopes. While edifice II has a summit depression, no such feature can be discerned on edifice I; the mountain appears to have a sharp peak.

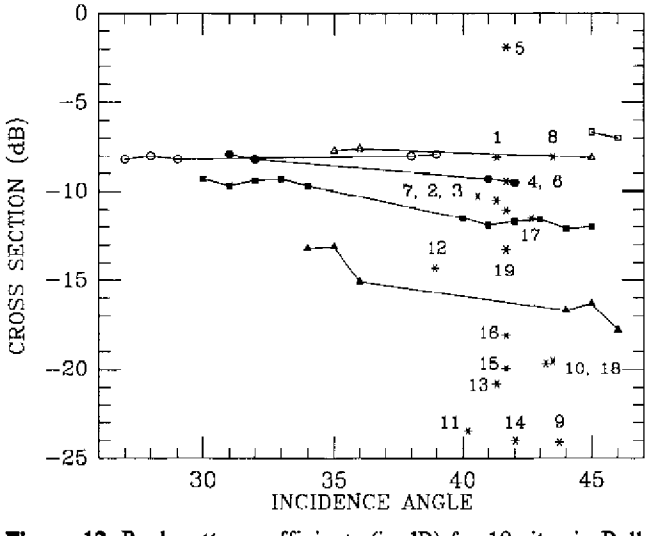

Figure 12. Backscatter coefficients (in dB) for 19 sites in Bell Regio (**Table 1**), Figure 11), shown as asterisks, and for six Kilauea Volcano lava flows. Kilauea data shown are interpolated from 5.6-cm and 24-cm AIRSAR measurements. Three a'a flows are shown by open symbols; the other three flows are pahoehoe texture. Note that the plains units and dark diffuse deposit have considerably lower cross sections than a smooth Hawaiian basalt.

There is a strong radar echo from the east flank of Tepev Mons, consistent with the rapid rise in topography along this side of the mountain (Figure 7c). *Barsukov et al.* [1986] noted the presence of a radar-bright region at the top of Tepev Mons and suggested that it might be a pyroclastic deposit blown west by the prevailing winds. Given the very high Magellan backscatter cross section for this area and its elevation (>6053.0-km radius), this bright annulus is more likely due to the presence of high-dielectric mineral phases [*Klose et al.*, 1992]. In the Venera data, there is a nearly square region of high backscatter surrounding the western caldera. Magellan data show the same western halo, but with a nested very bright region adjacent to the crater rim (Figure 7a), and a more complete annulus of bright material surrounding the eastern caldera. This difference in behaviors may represent variations in roughness within the summit deposits, with the eastern region being rough enough to reduce its radar echo at 10° incidence angle despite enhanced Fresnel reflectivity. The floor of the eastern caldera is very dark in the Venera image, suggesting a surface which is either rough at the scale of the radar wavelength or which is covered by a layer of unconsolidated material.

Magellan Emissivity Analysis

Magellan collected measurements of the microwave emission from the surface during a brief period between each

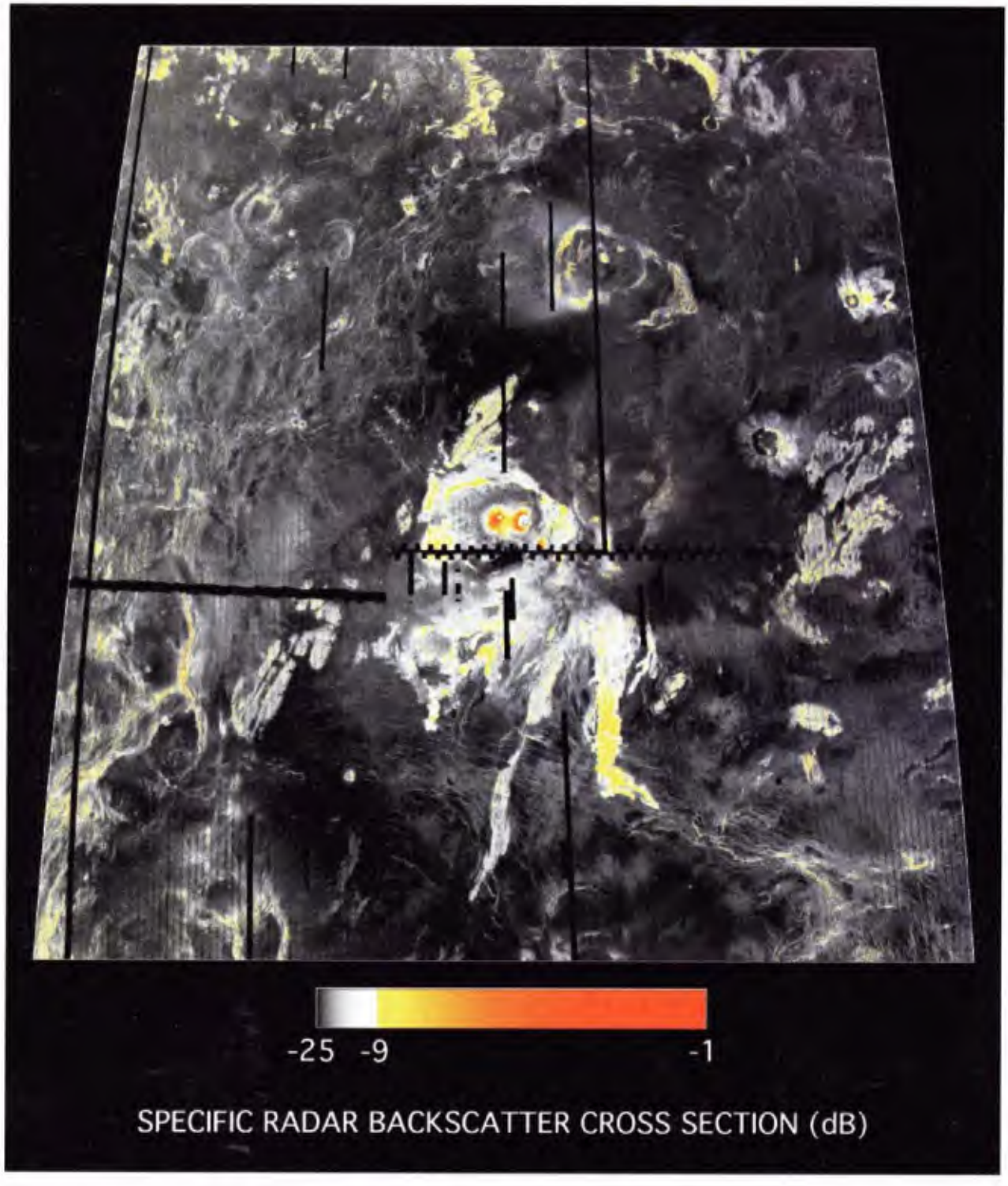

Plate 2. Color-coded Magellan backscatter image. Areas with backscatter coefficient (σ_0) greater than -9 dB are shown as shades of yellow to red. Note the lack of very strong radar backscatter enhancement from the two Tepev Mons calderas, in contrast to the high returns from other areas above 6053.0-km radius. Three large lava flows and a number of smaller patches are consistent with the roughness of Hawaiian a'a surfaces. Most other bright returns are associated with tessera units, crater ejecta blankets, or ridge structures.

group of SAR pulses. These observations can be processed using a model for the surface temperature to derive values for emissivity [*Pettengill et al.*, 1992]. The spatial resolution of the radiometer data varies with the spacecraft altitude, and is approximately 23x33 km over Bell Regio. In this section, we use the Magellan SAR and emissivity data to characterize changes in dielectric properties across the region as a guide to the bulk porosity and chemistry of the surface materials.

Analysis of global radiometer and SAR data has permitted a first-order model to be developed which relates the backscatter

Figure 13. Venera 15/16 radar image of Tepev Mons. Black arrows denote the eastern caldera and edifices 1 and 2. Image width ~475 km, centered on 29.7°N, 44.4°E. Topographic contours from Venera altimeter system. Incidence angle ~10°, with data processed through a high-pass filter which eliminates large-scale variations in backscatter intensity. Note the very low return from the eastern Tepev caldera and the bright echoes from the radar-facing sides of all three mountains.

and emissivity values for any given footprint to the dielectric constant ε and a surface roughness fraction (that portion of the surface covered by diffuse scattering elements) [*Campbell*, 1994]. This model works by assuming that the global mean correlation between backscatter and emissivity is due to roughness changes imposed on a single-dielectric material. The wind streaks noted in the geologic discussion above should not affect the results of this modeling, but extensive deposits of loose material should exhibit a lower dielectric constant than solid rock of the same composition.

We can use the model described above and two other methods to estimate dielectric constants on Venus (Plate 3). The model-derived roughness fraction and dielectric constant are shown in Plates 3a and 3b. Alternatives are to (1) ignore surface roughness and solve for ε from the plane-interface expression for horizontal-polarized emission (Plate 3c) or (2) use the altimeter-derived corrected reflectivity values (Plate 3d). The corrected reflectivity values, derived from Hagfors modeling of altimeter data, show a strong correlation with roughness, and yield much lower estimates of the dielectric constant atop Tepev Mons than those produced from the emissivity data. The discrepancies in the two estimates of ε may be due to the use of the Hagfors model and a subsequent roughness correction; this model is less valid at high surface roughnesses or in regions of mixed terrain types [*Pettengill et al.*, 1988; *McCollom and Jakosky*, 1993]. Estimates of ε made with the plane-interface assumption for emissivity also tend to be correlated with roughness, as evidenced by the lower dielectric constants found on tessera surfaces, lava flows, and crater ejecta blankets. The SAR/emissivity model suppresses the contribution of roughness to emissivity, so we will use the values shown in Plate 3b for our interpretations.

The dielectric constant over the Tepev Mons summit reaches a maximum value of 35, consistent with a loaded dielectric material [*Klose et al.*, 1992]. The areas of highest dielectric constant are located near the western caldera. Although it is well above the altitude associated with high-reflectivity deposits, the eastern caldera floor does not appear to have a dielectric constant above ~7. Permittivity values of 9-12 are found near the tops of the two small edifices and on the raised southwest rim of the eastern volcanic center. The dielectric constants of the relatively youngest lava flows tend to be slightly higher than those of older materials; this difference may be due to changes in rock chemistry with exposure to the atmosphere, development of a thin regolith with age, or to chemical differences between the original magmas. The roughness map (Plate 3a) shows that the Tepev Mons summit area is relatively smooth except for two rough annular patches surrounding the calderas.

A halo of smooth material with ε=6-7 surrounds Nefertiti corona, evidently produced by the crater Miriam. This deposit forms a roughly parabolic shape open to the west, similar to the low-emissivity crater parabolas studied by *Campbell et al.* [1992]. The Miriam parabola is not obvious on the SAR image; only a few small dark patches can be identified. There is a radar-bright area central to the parabola, and the model-derived dielectric constant for this material is similar to that of the plains. Since the parabolic deposit is evidently quite thin, we conclude that the ejecta must contain materials with quite high permittivities to offset the normal drop in dielectric constant with lower density [*Ulaby et al.*, 1988]. The occurrence of high-dielectric materials in crater ejecta may be due to impact melting and recondensation of the target rock [*Schultz*, 1992; *Campbell*, 1994].

There are several regions of lower dielectric constant (ε=2-3): a group of elongate SW-NE trending patches in the plains northwest of Tepev Mons and the triangular *dd* region. According to the model, all of these deposits are slightly rougher than the typical plains (Plate 3a). These roughness values may indicate that the fine-grained material, which we assume produces the lower values of ε, is not deep enough to completely mantle the surface roughness, and has instead collected in local flat areas. The low-dielectric area associated with unit *dd* extends west beyond the boundary mapped from the SAR data, showing that the emissivity information can be used to map thin surficial deposits. Such a signature might be caused by wind transport of an originally localized deposit of pyroclastic material or ejecta from a dark crater splotch (since no crater is evident). A pyroclastic deposit may only form on Venus in eruptions with high volatile contents [*Garvin et al.*, 1982; *Head and Wilson*, 1986], but the shape and mantling nature of this deposit do suggest the possibility of such an origin.

Magellan RMS Slope Analysis

Values of rms slope are derived from the Magellan altimeter radar echoes using the Hagfors model for quasi-specular scattering (Figure 14); the mean rms slope across the planet is 2.84° [*Ford and Pettengill*, 1992]. If we plot the average rms slope as a function of σ_o over the study region, there is an obvious correlation between the two measurements (Figure 15). This indicates that changes in surface roughness at the tens of meters scale (rms slope) are typically accompanied by similar changes in the centimeter-meter scale roughness that modulates the SAR echo at this incidence angle. Beyond a radar brightness of about -8 dB (at ~40°), there is little correlation between SAR backscatter and rms slope, presumably because the Hagfors model is no longer appropriate at these roughness scales. The close correspondence between SAR backscatter and rms slope implies that the changes in plains roughness, which dominate the mean curve because they are the most areally extensive

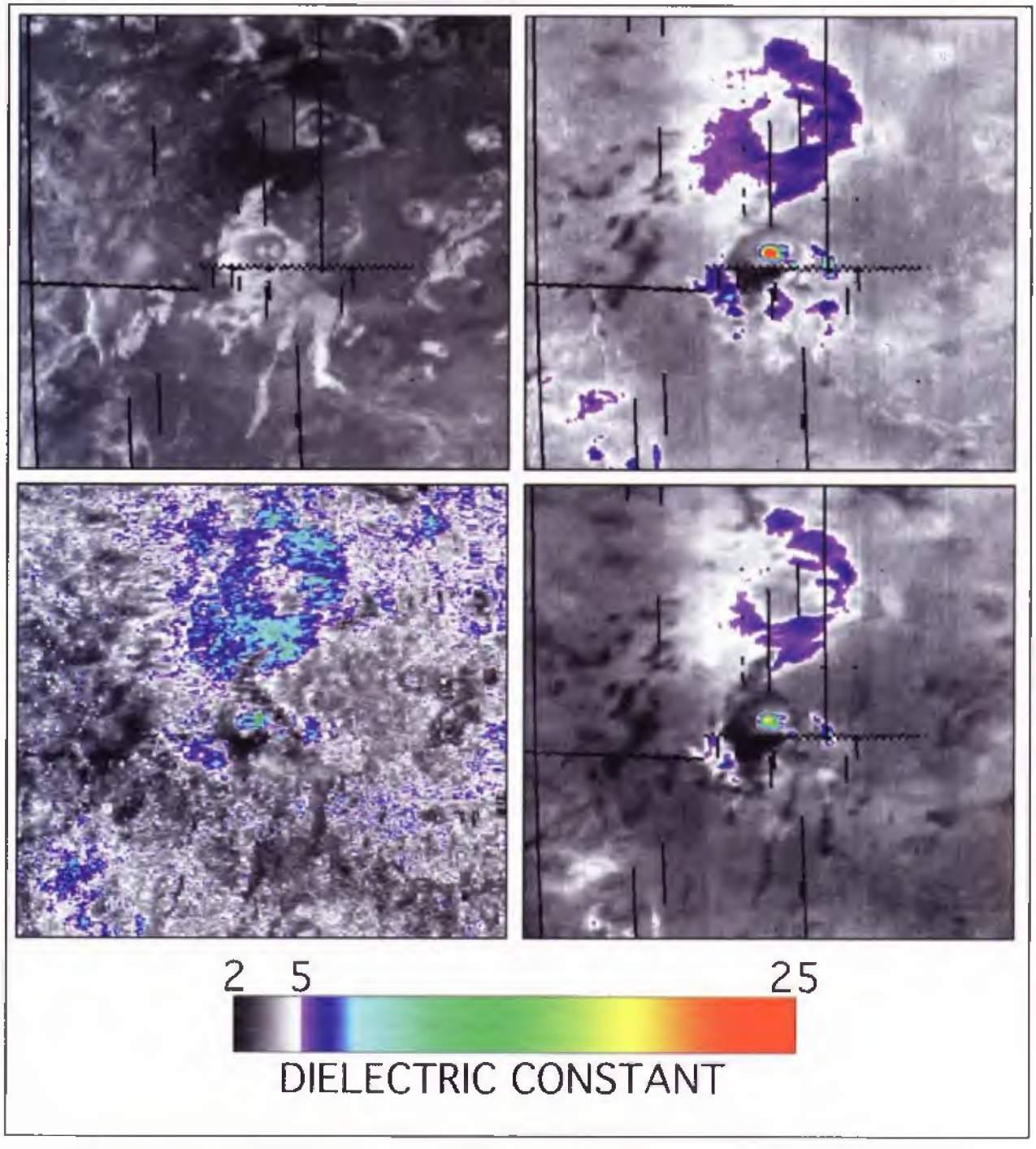

Plate 3. Roughness and dielectric constant model results for Bell Regio. Clockwise from upper left (a) Roughness (black=0, white =100%). (b) Model-derived dielectric constant. (c) Dielectric constant derived by using plane-surface horizontal emission model. (d) Hagfors corrected reflectivity converted to dielectric constant. Cylindrical projection for the area between 18°-42°N, 32°-58°E.

unit, typically occur simultaneously over a broad range of spatial scales (i.e., there are few cases where the meter-scale rubble increases without a similar rise in large surface undulations).

Campbell and Garvin [1993] calculated rms slopes for three Hawaiian lava flows (two pahoehoe and one a'a) from 80-120 m surface profiles. This analysis found that values of 1-2° are typical for smooth areas. Many of the plains units and edifice lava flows in the study area fall within this range (Table 1), consistent with the earlier interpretation of their roughness based on SAR data. There are a few exceptions to this general behavior. More recent lava flows from the eastern volcanic center (*f*2) are typically higher in rms slope than those of Unit 1, though this latter unit is brighter in backscatter.

The nature of the surface material within the eastern Tepev Mons caldera, where SAR images show a smooth surface

Figure 14. Image of rms slope data for Bell Regio from the global average data set (~5-km resolution). Sinusoidal projection of the area between 18°-42°N, 32°-58°E. Image stretch (black=0°, white=7°).

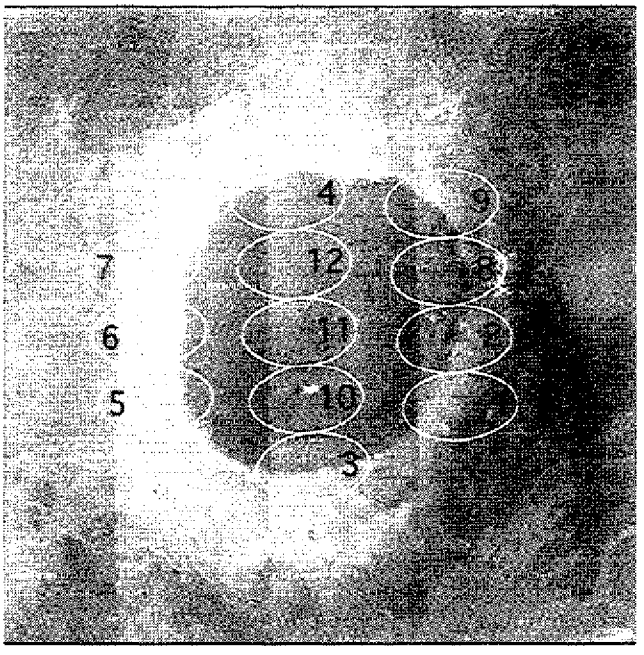

Figure 16. High-resolution (75-m pixels) SAR image of Tepev Mons east caldera (31-km diameter) with footprint ovals for the 12 altimeter traces shown in Figure 17. Note the ring of darker returns along the east and south edges of the caldera, which may indicate a gentle slope from the rim to the floor, and the small pits in the floor itself.

texture even at the full-resolution 75-m pixel scale (Figure 16), is also of interest. Despite the apparently smooth surface, three altimeter footprints (10-12 in Figure 16) which fall fully within the caldera have very poor specular peaks, and the Hagfors model yields rms slopes as high as 9°. Footprints which fall outside the caldera typically have rms slopes of ~3°. Given the Venera observation of low returns near 10° incidence angle for this surface, it seems likely that the eastern caldera floor is covered by a fine-grained deposit. This would account for both the moderate-low backscatter return (echoes coming largely from volume scattering within the soil, enhanced to some degree by elevated permittivity) and the high Hagfors rms slope (since volume scattering within the regolith will tend to spread the returned power over a larger range of angles).

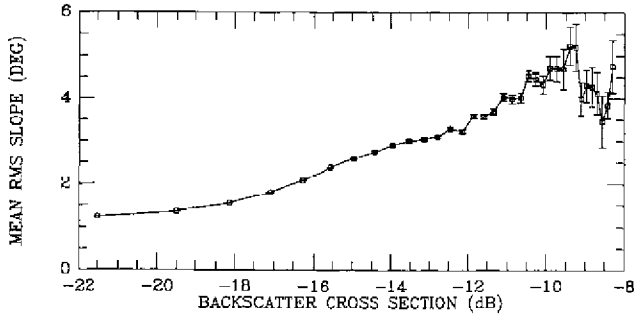

Figure 15. Magellan mean rms slope versus radar backscatter coefficient. Area covered is between 18°-42°N, 32°-58°E. Slope data from global data set, SAR data from unfocused backscatter measurements in raw radiometer data records. Error bars show one standard deviation for rms slope distribution.

Magellan Altimeter Analysis: Structure of the Tepev Mons East Caldera

The structure of volcanic calderas can provide information on magma chamber depth and eruption styles. In order to study the spatial variation of topography around the Tepev Mons eastern caldera, we analyzed the individual Magellan altimeter echo profiles. These data are stored as 302 measurements of backscatter power at time intervals of 221 μs, in both range-unsharpened and range-sharpened forms. The latter data have been corrected (by time-shifting each look) for the change in spacecraft position across the ~20 looks which form each profile [*Ford and Pettengill*, 1992]. The resampled global topography data record (GTDR) data set has a spatial resolution of ~5 km, but the weighted averages used to produce these values may suppress or misrepresent topographic variations in areas of rapidly varying elevation (crater rims, calderas, ridges, etc.) or in very rough terrains.

We analyzed plots of echo power versus radius for 12 altimeter footprints which cross the eastern caldera of Tepev Mons (Figure 16). These are divided into two groups based on the relative strength of the backscatter in each profile (Figure 17). Figure 17a shows the profiles which appear to have sampled the highly reflective terrain around the rim of the caldera, while Figure 17b shows those points which either fell entirely within the interior or did not receive a strong echo from the rim deposit. From these data, we estimate that the floor of the caldera is at nearly the same topographic level (to within a few hundred meters) as the rim. The earliest echoes in Figure 17b occur at approximately 6056.5-km radius, very similar to the echo peaks seen in Figure 17a (note in particular the upper three footprint traces). There is some evidence on the highest resolution SAR images for a gentle slope along

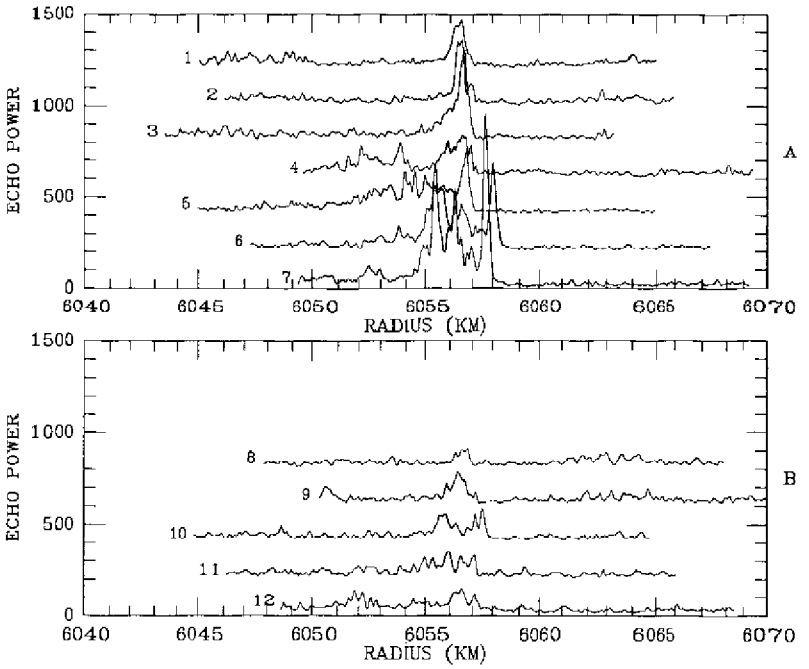

Figure 17. Magellan altimeter footprint echo traces (range-sharpened) for Tepev Mons summit. Numbers on each profile correspond to numbered ovals in Figure 16. (a) Seven footprints which appear to sample the highly reflective terrain surrounding the eastern caldera. Note the large peak at early time (large elevation) in profiles 6 and 7. (b) Five footprints which fall within the eastern caldera. There is no large difference in first return (elevation) between these points and those in Figure 17a. Note the low returned power and highly time-spread echo of these points.

the interior walls of the caldera, but the existing altimeter data do not provide sufficient detail to resolve further the difference in rim and floor height. Two footprints (6, 7) show a strong early return which might be interpreted as an elevated portion of the western rim lying 1000-1500 m higher than the rest of the rim and floor. There is no evidence for such a dramatic topographic scarp on the full-resolution SAR image of this region (Figure 16), so these two echo peaks are problematic. The possibility that these are the only measurements of the rim crest itself, and in all other footprints the strong return is from the caldera floor, seems unreasonable. These results demonstrate that caution is required when using single Magellan altimeter measurements for small-scale studies, since surface roughness and off-nadir scatterers may play a major role in determining the shape of the final echo.

Summary of Results

This work utilizes a number of techniques for linking terrestrial observations or theoretical models to Magellan data, and demonstrates the value of integrating geologic mapping with quantitative analyses. Mapping based on Magellan SAR images shows that Bell Regio is comprised of lava flows from at least five major volcanic sources (Tepev Mons, Nefertiti corona, a large unnamed shield east of Tepev, and two small edifices southeast of Tepev). The volcano Api Mons and several coronae, all with large flow fields, surround the upland. The region has not been influenced by large-scale rifting, and the dominant tectonic features are circumferential fractures surrounding Tepev Mons and the volcano to its east. The lack of a rift zone distinguishes this uplift from Western Eistla, Atla, and Beta Regiones, all of which have volcanism connected with extensive rifting. The lava flows in this region are divided into five major geologic units (*f1-f5*) based on distinct differences in radar brightness, morphology, superposition, or cross-cutting relationships, and the surrounding plains are divided into three general types (*dp, lp, and rp*).

Quantitative analysis of the Magellan and Venera data are used to augment the general geologic framework based on the SAR mapping and for more detailed local-area studies. These data are useful for identifying and characterizing the nature of anomalous areas and for placing Venus geologic units in a terrestrial context. Only three large lava flows have surface textures similar to those of terrestrial a'a, implying that most of the deposits were emplaced at relatively low effusion rates (<100 m^3/s over small fissure lengths) over long periods of time [*Rowland and Walker*, 1990]. A'a-type flows may represent volume eruption rates on the order of several hundred to 1000 m^3/s. Alternatively, the magma which produced the smooth flows may have been less viscous than typical Hawaiian lavas. A lava flow from one of two unnamed edifices, which appears to predate many of the volcanic deposits in Bell Regio, has a surface texture which is uncommon on Venus. The flow has a knobby or ridged morphology which protrudes through later lavas, indicating a surface with many meters of relief. This may be an example of high-viscosity lava, similar to festoon flows found elsewhere, or of tumuli formed by slow inflation of a flow field.

High dielectric deposits occur in most areas above 6053-km radius, presumably due to the accumulation of high Fresnel-reflectivity materials which are in equilibrium with the

atmosphere at these altitudes [*Klose et al.*, 1992]. Magellan emissivity and SAR data, as well as Venera images, show that there are variations in texture within the summit region of Tepev Mons, with the rough materials confined to annular regions surrounding the two calderas. The highest values of permittivity (~35) are found on the western portion of the Tepev Mons summit, though neither caldera floor appears to have strongly enhanced dielectric values. The study of the Tepev Mons eastern caldera is a good example of the value of integrating all available data sets. This caldera, and its neighbor to the west, appear to be very shallow, perhaps due to infilling by lava flows after the most recent collapse events. The eastern caldera floor is also characterized by moderate radar brightness at 40°, very low brightness at 10°, and high Hagfors-model rms slopes. These observations imply a surface with a porous covering of ash or soil.

Impact craters have produced several intriguing features. A parabolic region of low emissivity surrounding Nefertiti corona is interpreted as evidence for a thin mantling deposit with enhanced dielectric constant (6-7), which is not evident in the SAR image except as small discontinuous dark patches. These properties are similar to those of type *pe* parabolas studied by *Campbell et al.* [1992], so the 13-km crater Miriam is the likely source for this large halo. Fine-grained material from Potanina and Miriam is also found as wind streaks near tessera or plains ridges, and in some cases has piled up against these obstacles. A triangular low-dielectric region south of the summit of Tepev Mons may also be crater ejecta, but the lack of any central bright area leaves open the possibility of a wind-transported pyroclastic deposit.

The available data show that Bell Regio has undergone a wide range of volcanic processes whose characteristics have shifted over time. The initial phase of volcanism from the eastern volcanic center produced a low-relief shield with a central region analogous to some corona structures, and relatively smooth lava flow fields. The presence of tessera blocks with similar deformation patterns surrounding the volcanic uplands may indicate that the rising plume of hot material which supplied the magma for these eruptions impinged on the base of a large tessera region and subsequently buried much of it. Contemporaneous or later eruptions from Tepev Mons and the two small edifices produced volcanoes with high flank slopes (up to 40°), rougher lava flow surface textures, and at least two steep-sided domes. The steeper slopes may indicate the eruption of more silicic magma from a differentiated source such as a chamber in the crust. Nefertiti corona also erupted a significant amount of lava, but the relationship of the magma source for this feature to those of the other large vent areas is uncertain. Late-stage activity at Tepev Mons produced an apparent ash deposit within the eastern caldera and perhaps the radar-dark material on the south flank. The absence of rifting in this area suggests that volcanism was driven largely by upwelling material from the mantle (as opposed to shallow melting in response to tectonic activity), and that this plume did not exploit a pre-existing region of high extensional stresses to reach the surface.

Acknowledgments. This work was supported in part by Planetary Geology and Geophysics grant NAGW-3360 and by funds from the Venus Data Analysis Program. The authors thank D. Senske and B. R. Hawke for thorough and insightful reviews, and R. Craddock and J. Zimbelman for helpful discussions.

References

Arvidson, R.E., R. Greeley, M.C. Malin, R.S. Saunders, N. Izenberg, J.J. Plaut, E.R. Stofan, and M.K. Shepard, Surface modification of Venus as inferred from Magellan observations of plains, *J. Geophys. Res.*, *97*, 13,303-13,318, 1992.

Barsukov, V.L., et al., The geology and geomorphology of the Venus surface as revealed by the radar images obtained by Veneras 15 and 16, *Proc. Lunar Planet Sci. Conf. 16th, Part 2, J. Geophys. Res., 91, suppl.*, D378-D398, 1986.

Campbell, B.A., Merging Magellan emissivity and SAR data for analysis of Venus surface dielectric properties, *Icarus*, in press, 1994.

Campbell, B.A., and D.B. Campbell, Analysis of volcanic surface morphology on Venus from comparison of Arecibo, Magellan, and terrestrial airborne radar data, *J. Geophys. Res.*, *97*, 16,293-16,314, 1992.

Campbell, B.A., and J.B. Garvin, Lava flow topographic measurements for remote sensing data interpretation, *Geophys. Res. Lett.*, *20*, 831-834, 1993.

Campbell, B.A., and R.C. Kozak, Gravity analysis of Bell Regio, Venus from Pioneer-Venus and Venera data (abstract), *Lunar Planet. Sci. Conf., XIX*, 158-159, 1988.

Campbell, D.B., N.I.S. Stacy, W.I. Newman, R.E. Arvidson, E.M. Jones, G.S. Musser, A.Y. Roper, and C. Schuller, Magellan observations of extended impact crater related features on the surface of Venus, *J. Geophys. Res.*, *97*, 16,249-16,278, 1992.

Ford, P.G., and G.H. Pettengill, Venus topography and kilometer-scale slopes, *J. Geophys. Res.*, *97*, 13,102-13,114, 1992.

Garvin, J.B., J.W. Head, and L. Wilson, Magma vesiculation and pyroclastic volcanism on Venus, *Icarus*, *52*, 365-372, 1982.

Greeley, R., et al., Aeolian features on Venus: Preliminary Magellan results, *J. Geophys. Res.*, *97*, 13,319-13,346, 1992.

Head, J.W., and L. Wilson, Volcanic processes and landforms on Venus: Theory predictions, and observations, *J. Geophys. Res.*, *91*, 9407-9446, 1986.

Janle, P., D. Jannsen, and A.T. Basilevsky, Morphologic and gravimetric investigations of Bell and Eisila Regiones on Venus, *Earth Moon Planets*, *39*, 251-273, 1987.

Janle, P., D. Jannsen, and A.T. Basilevsky, Tepev Mons on Venus: Morphology and elastic bending models, *Earth Moon Planets*, *41*, 127-139, 1988.

Klose, K.B., J.A. Wood, and A. Hashimoto, Mineral equilibria and the high radar reflectivity of Venus mountaintops, *J. Geophys. Res.*, *97*, 16,353-16,370, 1992.

Konopliv, A.S., N.J. Borderies, P.W. Chodas, E.J. Christensen, W.L. Sjogren, B.G. Williams, G. Balmino, and J.P. Parriot, Venus gravity and topography: 60th degree and order model, *Geophys. Res. Lett.*, *20*, 2403-2406, 1993.

McCollom, T.M., and B.M. Jakosky, Interpretation of planetary radar observations: The relationship between actual and inferred slope distributions, *J. Geophys. Res.*, *98*, 1173-1184, 1993.

McGovern, P.J., and S.C. Solomon, Estimates of elastic plate thickness beneath large volcanoes on Venus, International Colloquium on Venus, *LPI Contrib.*, *789*, 68-70, 1992.

Moore, H.J., J.J. Plaut, P.M. Schenk, and J.W. Head, An unusual volcano on Venus, *J. Geophys. Res.*, *97*, 13,479-13,494, 1992.

Pettengill, G.H., P.G. Ford, and B.D. Chapman, Venus: Surface electromagnetic properties, *J. Geophys. Res.*, *93*, 14,881-14,892, 1988.

Pettengill, G.H., P.G. Ford, and R.J. Wilt, Venus surface radiothermal emission as observed by Magellan, *J. Geophys. Res.*, *97*, 13,091-13,102, 1992.

Rowland, S.K., and G.P.L. Walker, Pahoehoe and a'a in Hawaii: Volumetric flow rate controls the lava structure, *Bull. Volcanol.*, *52*, 615-628, 1990.

Saunders, R.S., et al., Magellan mission summary, *J. Geophys. Res.*, *97*, 13,067-13,090, 1992.

Schultz, P.H., Atmospheric effects on ejecta emplacement and crater formation on Venus from Magellan, *J. Geophys. Res.*, *97*, 16,183-16,248, 1992.

Senske, D.A., G.G. Schaber, and E.R. Stofan, Regional topographic rises on Venus: Geology of Western Eistla Regio and comparison to Beta Regio and Atla Regio, *J. Geophys. Res., 97*, 13,395-13,420, 1992.

Smrekar, S.E., Interpretation of Magellan gravity data for large volcanic swells on Venus: Implications for interior structure (abstract), *Lunar Planet. Sci. Conf., XXV*, 1295-1296, 1994.

Smrekar, S.E., and R.J. Phillips, Venusian highlands: Geoid to topography ratios and their implications, *Earth Planet Sci. Lett., 107*, 582-597, 1991.

Solomon, S.C., et al., Venus tectonics: An overview of Magellan observations, *J. Geophys. Res., 97*, 13,199-13,256, 1992.

Stofan, E.R., V.L. Sharpton, G. Schubert, G. Baer, D.L. Bindschadler, D.M. Janes, and S.W. Squyres, Global distribution and characteristics of coronae and related features on Venus: Implications for origin and relation to mantle processes, *J. Geophys. Res., 97*, 13,347-13,378, 1992.

Theilig, E., and R. Greeley, Lava flows on Mars: Analysis of small surface features and comparisons with terrestrial analogs, *Proc. Lunar Planet. Sci. Conf., Part 1, J. Geophys. Res., 91, suppl.*, E193-E206, 1986.

Ulaby, F.T., T. Bengal, J. East, M.C. Dobson, J. Garvin, and D. Evans, Microwave dielectric spectrum of rocks, *Rep. 23817-1-T*, 81 pp., Univ. of Mich. Radiation Lab., Ann Arbor, 1988.

B.A. Campbell, Center for Earth and Planetary Studies, National Air and Space Museum, Washington, D.C. 20560.

P.G. Rogers, Solar System Exploration Division, NASA Headquarters, Washington, D.C. 20546.

(Received November 29, 1993; revised May 6, 1994; accepted July 15, 1994.)